

ROSAT X-RAY OBSERVATIONS OF THE COOLING FLOW CLUSTER A2597

CRAIG L. SARAZIN

Department of Astronomy, University of Virginia,
P.O. Box 3818, Charlottesville, VA 22903-0818;
cls7i@virginia.edu

AND

BRIAN R. MCNAMARA

Harvard-Smithsonian Center for Astrophysics,
60 Garden Street, Cambridge, MA 02138;
brm@cfa241.harvard.edu

ABSTRACT

The cluster A2597 was observed in X-rays with the ROSAT PSPC and HRI detectors. The X-ray emission from the cluster extends out to a radius of at least 2.37 Mpc. The X-ray isophotes are oriented similarly to the optical isophotes of the central cD galaxy and to the isopleths of the galaxy distribution in the cluster, but are otherwise quite regular, suggesting that this cluster is reasonably relaxed and in hydrostatic equilibrium. The merged HRI and PSPC surface brightness profile is not adequately fit by a beta model because of the central X-ray surface brightness peak, indicating the presence of a cooling flow. If the central 108 arcsec in radius are excluded, an acceptable fit is found which gives $\beta = 0.64^{+0.08}_{-0.03}$ but only an upper limit to the core radius, $r_{core} < 78$ arcsec. The gas density and accumulated mass were derived as a function of radius, and the hydrostatic equilibrium condition was used to determine the total gravitational mass, also as a function of radius. Within a radius of 2 Mpc, we found masses of $M_{gas} = 1.2 \times 10^{14} M_{\odot}$ and $M_{tot} = 6.5 \times 10^{14} M_{\odot}$, and a gas mass fraction of about 19%. However, our poor knowledge of the spatial variation of the gas temperature makes the total mass values uncertain by at least a factor of two.

The ROSAT PSPC X-ray spectrum of the cluster was determined. Both the overall cluster spectrum and the spatially resolved spectra within 300 kpc require the presence of both hot gas and a cooling flow in the spectrum. The spectrally determined total cooling rate of $\dot{M} = 344^{+75}_{-67} M_{\odot} \text{ yr}^{-1}$ is in good agreement with those derived from analyses of the X-ray surface brightness profile from the *Einstein* IPC and the ROSAT HRI images. The ROSAT spatially resolved X-ray spectra indicate that the cooling component is distributed over the inner ~ 300 kpc in radius of the cluster. The presence of the cooling flow in the central regions and poorer statistics in the outer regions prevent us from deriving an accurate profile for the variation of the ambient cluster gas temperature.

We do not detect any significant excess X-ray absorption toward the center of A2597, and we set a very conservative upper limit on the excess column in front of the cooling flow region of $\Delta N_H < 1.72 \times 10^{20} \text{ cm}^{-2}$. A2597 is one of the few cooling flows toward which a large column has been detected in radio observations (O'Dea et al. 1994a). A total column of $N_H \approx 1 \times 10^{21} \text{ cm}^{-2}$ was seen in 21 cm absorption against the very small central radio source. Our X-ray upper limit is not inconsistent with the 21 cm detection if the absorber only covers the small region (~ 6 arcsec) occupied by the radio source. However, we can rule out an absorber with a uniform column which covers the entire cooling flow, or even just the smaller region of the extended optical emission line nebula.

Subject headings: cooling flows — galaxies: clusters: general — galaxies: clusters: individual (A2597)
— galaxies: cD — intergalactic medium — X-rays: galaxies

1. INTRODUCTION

The Abell richness class 0 cluster A2597 (Abell, Corwin, & Olowin 1989) at a redshift of $z = 0.0852$ is elliptical but quite regular in its galaxy and gas distributions (e.g., Trèvese et al. 1992b; Buote & Tsai 1996), with an elongated cD galaxy at its center (McNamara & O'Connell 1993). This central galaxy in A2597 contains the moderately luminous ($P_{20} = 5.98 \times 10^{25} \text{ W/Hz}$) radio source PKS 2322-122 (Owen, White, & Burns 1992; Ball, Burns, & Loken 1993). Recent radio observations show that this very small source ($\lesssim 6$ arcsec in diameter) has emission

from a radio core, a strongly bent jet, and two steep spectrum radio lobes on either side of the nucleus (Sarazin et al. 1995b, hereafter Paper I).

A2597 is a powerful X-ray source with a total luminosity of $L_X = 6.45 \times 10^{44} \text{ erg s}^{-1}$ (2–10 keV; David et al. 1993). The cluster contains a strong central cooling flow (Crawford et al. 1989; Paper I), with a total cooling rate of $\dot{M} \approx 300\text{--}400 M_{\odot} \text{ yr}^{-1}$ out to a radius of $r_c \approx 200$ kpc. As is often true of strong cooling flows, the central cD galaxy in A2597 has extensive optical and UV line emitting filaments (Hu 1988; Heckman et al. 1989; Crawford & Fabian 1992). The X-ray emission in the central re-

gions is elongated along a direction which is perpendicular to the orientation of the radio lobes (Paper I). Similar X-ray—radio anti-correlations have been seen in a number of other cooling flow clusters (e.g., Böhringer et al. 1993; Harris, Carilli, & Perley 1994; Sarazin, Baum, & O’Dea 1995a).

As is also true of the central galaxies in many other cooling flow clusters, the central optical colors of the cD galaxy in A2597 are considerably bluer than a typical giant elliptical galaxy (Crawford & Fabian 1992; McNamara & O’Connell 1993). The bluest regions lie in lobe-like structures which extend radially $\sim 5 - 7$ kpc on either side of the I-band nucleus with a NE/SW orientation (McNamara & O’Connell 1993). These blue optical lobes appear to be oriented along the axis of the radio jets in the central galaxy (Paper I). The optical lobes could originate from a number of processes. However, the most plausible on morphological and energetic grounds are radio-lobe-induced star formation or scattered nonthermal radiation beamed anisotropically from the nucleus (e.g., Paper I). There is also evidence for the presence of dust in the central regions from the optical color distribution in the cD galaxy and from the ratio of H α /Ly α line emission (Hu 1992; McNamara & O’Connell 1993).

Through a re-analysis of *Einstein* Solid State Spectrometer X-ray spectra of the central regions of cooling flow clusters, White et al. (1991) found evidence for very large amounts of excess soft X-ray absorption. A2597 was not included in the sample studied by White et al. However, for strong cooling flows like A2597, the excess columns were typically $\gtrsim 1 \times 10^{21} \text{ cm}^{-2}$. ROSAT PSPC and ASCA spectra have confirmed this absorption in a number of clusters (Allen et al. 1993; Fabian et al. 1994), and the ROSAT PSPC spectral images have shown that the excess absorption is confined to the inner cooling regions of the cluster in several cases (Allen et al. 1993; Irwin & Sarazin 1995). In general, the cold material producing this absorption has not been detected at non-X-ray wavelengths, despite considerable efforts (e.g., McNamara & Jaffe 1993; Antonucci & Barvainis 1994; O’Dea et al. 1994b; Voit & Donahue 1995).

A2597 is an exception to this. O’Dea et al. (1994a) detected 21 cm H I absorption toward the central radio source in the cD galaxy at the center of the cooling flow. The total column is $N_H \approx 1 \times 10^{21} \text{ cm}^{-2}$, which is comparable to the columns derived from X-ray spectra of other cluster cooling flows. The absorber has a component which is extended at least over the rather small diameter of the radio source (~ 6 arcsec). Unfortunately, there is no X-ray-derived absorbing column for this cluster with which to compare the 21 cm detection. The Galactic column toward the cluster is relatively small ($N_H = 2.45 \times 10^{20} \text{ cm}^{-2}$; Stark et al. 1992), making the detection of a large column of excess X-ray absorption, if present, straightforward.

We have observed A2597 with both the ROSAT High Resolution Imager (HRI) and Position Sensitive Proportional Counter (PSPC). The HRI results on the inner structure of the cooling flow and its relation to the radio source have already been presented in Paper I. In the present paper, we will concentrate on the results from the ROSAT PSPC. The purpose of these observations was to

use the high sensitivity of the PSPC to map the large-scale X-ray emission of A2597 and to use the spectral resolution to determine the thermal structure of the cluster. In addition, the PSPC is an ideal instrument for searching for excess soft X-ray absorption, which we can compare to the radio detection of neutral hydrogen and to the excess absorption measurement toward other cooling flow clusters. The X-ray observations are described in § 2. The overall X-ray image is discussed in § 3. The X-ray spectrum of the cluster is analyzed in § 4, and the temperature structure is presented in §§ 4.1 and 4.2. We derive an upper limit on the excess X-ray absorption and compare to the radio observations in § 4.3. The shape of the X-ray emission and its radial profile are determined in §§ 5.1 and 5.2. These are used to determine the distribution of the gaseous and total gravitating mass in § 6. The results are summarized in § 7. Other X-ray sources in the field are listed in an Appendix.

All distance-dependent values in this paper assume $H_0 = 50 \text{ km s}^{-1} \text{ Mpc}^{-1}$ and $q_0 = 0.0$.

2. X-RAY OBSERVATIONS

The cluster was observed for 7243 seconds with the ROSAT Position Sensitive Proportional Counter (PSPC) on 27 November, 1991 (all of the final results presented here are based on the Rev. 2 version of the data) and with the ROSAT High Resolution Imager (HRI) for a total of 17,811 seconds. The HRI observation was done in two intervals: 6-8 December, 1991 and the second was 6-9 June, 1992. The structure of the cooling flow as seen in the ROSAT HRI data was discussed previously in Paper I, where the X-ray structure was compared to radio and optical structures at the cluster center. Here, we will concentrate on the PSPC data. We will only discuss the global properties of the HRI data which were not addressed in Paper I.

The PSPC data was screened for periods of high background based on a Master Veto Rate > 170 (Plucinsky et al. 1993), for other times of high background, for periods of 15 seconds after switching to the high voltage, and for periods with an uncertain aspect solution. The analysis was done with a combination of the IRAF/PROS software, the XSPEC/XANADU software, the XSELECT program, and Snowden’s SXRb package for the analysis of diffuse X-ray emission (Snowden 1995). The screened data contained a total exposure of 6721 seconds and the average Master Veto Rate was 87.25. The data were corrected for particle background, scattered solar X-ray background, the long term enhancements (LTE) in this background, and afterpulses. With these backgrounds removed, the image was corrected for exposure and vignetting.

The Appendix gives the image of the whole field of view of the PSPC observation (Figure 12 below), and a list of the field X-ray sources. We attempted to use optical identifications of these sources to check and improve the positions in the X-ray image. Unfortunately, the optical identifications are uncertain and do not lead to a simple, consistent transformation of the ROSAT coordinates which would improve the correspondence the optical coordinates. Similarly, the differences between the ROSAT HRI and PSPC positions of the point sources in common do not suggest a simple transformation of the HRI and

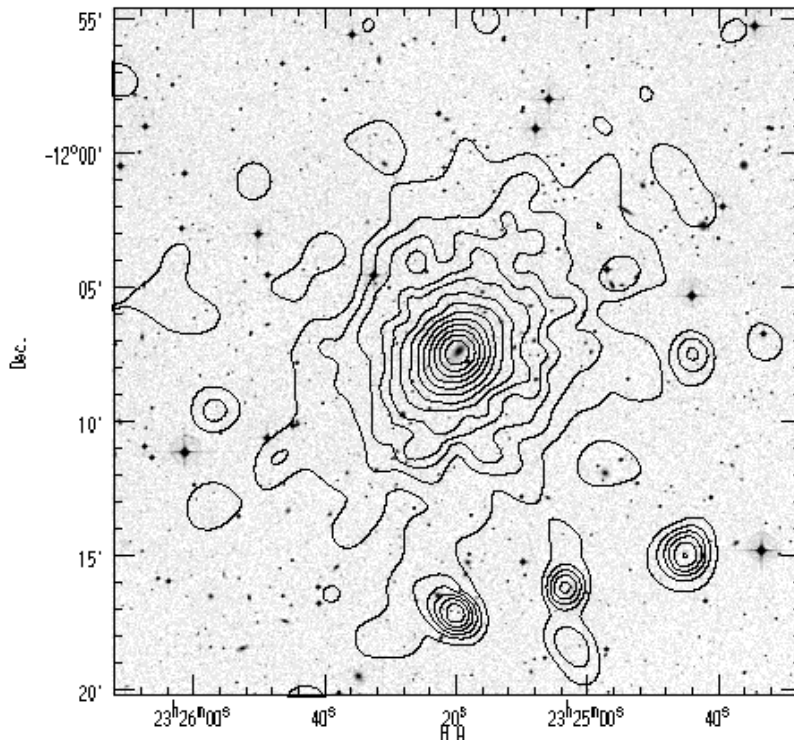


Fig. 1.— A contour plot of the X-ray surface brightness of the central 34 arcmin (4.4×4.4 Mpc) A2597 cluster. The X-ray contours are superposed on the optical image of the cluster from the Digitized Sky Survey. The contours are logarithmically spaced with five contours per dex, and the lowest contour corresponds to $0.0014 \text{ cts sec}^{-1} \text{ arcmin}^{-2}$ in the $0.4 - 2.4$ keV ROSAT band (PI channels 42–247). The image has been corrected for background, vignetting, and exposure, and adaptively smoothed to a signal-to-noise of five per smoothing beam. The coordinates are J2000.

PSPC coordinates to bring them into better agreement. In what follows, we will assume that the peak in the X-ray surface brightness of the A2597 cluster agrees with the nucleus of the central cD galaxy as determined from radio observations, R.A. = $23^{\text{h}}25^{\text{m}}19^{\text{s}}.64$ and Dec. = $-12^{\circ}07'27''.4$ (Paper I).

3. X-RAY IMAGE

Figure 1 shows the image of the X-ray emission from the central 34 arcmin (4.4×4.4 Mpc) of the cluster, superposed on the optical image of the cluster from the Digitized Sky Survey. The X-ray image was cleaned, background subtracted, exposure and vignetting corrected, and adaptively smoothed as discussed above. This image is restricted to the hard band on ROSAT of $0.4 - 2.4$ keV (PI channels 42–247). The cluster X-ray emission is quite hard, particularly away from the bright cooling flow region at the center. Restricting the emission to the hard band removes much of the background and emission by other sources, but does not affect the number of photons from the cluster as strongly.

4. SPECTRAL ANALYSIS

4.1. Global Spectra

The spectral resolution of the ROSAT PSPC allows the determination of the spectral properties of clusters, at least when the temperature is low or the observation contains a

sufficiently large number of photons. The only published spectral information on A2597 is from the Monitor Proportional Counter (MPC) on the *Einstein* Observatory, which provided a best-fit temperature of 9.1 keV with a 90% confidence lower limit of 3.8 keV (David et al. 1993). We analyzed the PSPC spectrum of A2597 using the facilities within PROS and XSPEC. We present the results obtained with XSPEC; the results of spectral fitting with PROS were generally consistent. Only counts in the photon energy range $0.11 - 2.1$ keV were used (PI channels 3–32). The two higher energy channels (PI channels 33 and 34) have uncertain calibrations and were excluded. All fitted spectral bins had >10 counts. The errors in the counts were determined from the square root of the number of photons; we did not use the PROS Poisson errors because these often result in unrealistically low values of the χ^2 statistic. Some of the results of the spectral fitting are summarized in Table 1. All of the errors or upper limits given for spectral parameters are at the 90% confidence level.

First, we determined the global spectrum of the cluster by extracting the counts from a circle of radius 1 Mpc (7.76 arcmin). The spectrum was corrected for particle and X-ray background using a circular annulus extending from 7.76 to 13.4 arcmin. The initial model we adopted for the spectrum was a Raymond-Smith model (Raymond & Smith 1977) for the thermal emission and the Wisconsin model (Morrison & McCammon 1983) for foreground Galactic absorption. We refer to this as a “single temper-

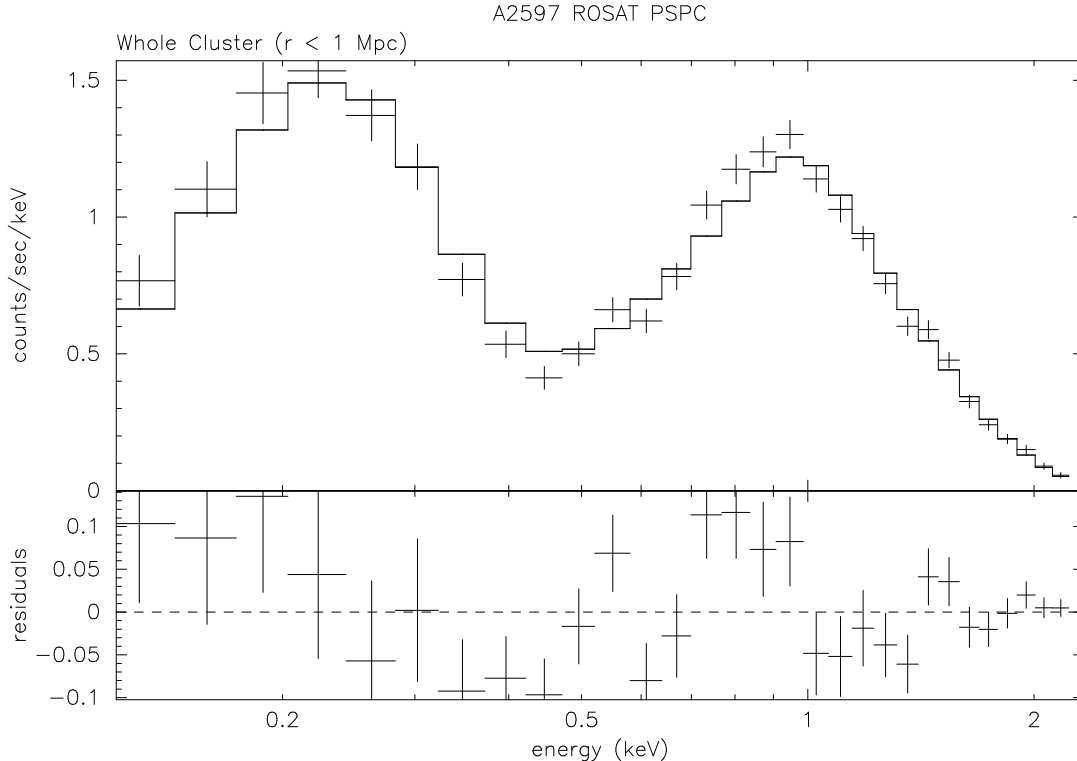


Fig. 2.— The ROSAT PSPC X-ray spectrum for the whole A2597 cluster ($r \leq 1$ Mpc) as a function of the measured photon energy is shown in the upper panel. The crosses give the data points with $1\text{-}\sigma$ error bars, while the histogram is the best-fit single temperature model (Table 1). The width of the data points or histogram steps is the width of the energy channels used to accumulate the data. The lower panel gives the residuals to the fit (in counts/sec/keV).

ature” model in Table 1 and in the following discussion. The best-fit single temperature model for the whole cluster spectrum had a temperature of $kT = 2.61^{+0.68}_{-0.48}$ keV, a hydrogen column density of $N_H = 1.89^{+0.21}_{-0.20}$ cm^{-2} , and a cosmic heavy element abundance fraction of $0.53^{+0.34}_{-0.21}$. Figure 2 shows the observed X-ray spectrum, the best-fit single temperature model, and the residuals to the fit. This is a poor fit, with a χ^2 of 47.88 for 26 degrees of freedom (d.o.f.).

The measured Galactic hydrogen column toward A2597 is $N_H = 2.45 \times 10^{20} \text{ cm}^{-2}$ (Stark et al. 1992). This is slightly larger than the column determined from the PSPC spectrum. In the region around A2597, the Galactic column varies by about $0.2 \times 10^{20} \text{ cm}^{-2}$, and it is likely that there are additional systematic uncertainties at least this large both in the determination of the Galactic column and in the X-ray determination of the column density (for example, PROS and XSPEC give slightly differing values.) Thus, the X-ray and radio determinations of the Galactic column are in reasonable agreement if systematic errors are included. The heavy element abundance is poorly determined, but is similar to the values generally found for X-ray clusters.

The best-fit temperature is incompatible with the temperature derived from the *Einstein* MPC. David et al. (1993) found a best-fit temperature of 9.1 keV with a 90% confidence lower limit of 3.8 keV. The PSPC temperature would also be lower than those typically found for clusters of this X-ray luminosity. These discrepancies and the poor

fit to a single temperature model suggest that the cluster has at least two temperature components in its spectrum. Most of the emission (particularly on the large scales sampled by the MPC) would be in a hard component, while a softer component would provide much of the flux in the PSPC band. The residuals in Figure 2 are also suggestive of additional soft X-ray emission. A model with two temperatures does provide an improved fit to the observations. The lower temperature is $kT = 1.04^{+0.09}_{-0.15}$ keV, while the higher temperature is poorly determined but considerably larger.

Previous *Einstein* IPC and ROSAT HRI images have shown that A2597 possesses a cooling flow at the center of the cluster (Crawford et al. 1989; Paper I). The cooling radius is approximately 100-250 kpc. Below, we show that the cooler spectral component is localized to the central regions of the cluster. Thus, it seems reasonable to attribute the cooler component in the spectrum of A2597 to this cooling flow, and to model it using the spectrum of gas cooling subject to its own radiation. A cooling flow spectrum should be reasonably approximated by isobaric cooling. We therefore added a component to the model with the spectrum of gas cooling isobarically from the ambient cluster gas temperature to a very low temperature. The initial temperature and abundances of this cooling flow component were assumed to be the same as that of the general intracluster gas. We refer to this as a “single temperature plus cooling flow” model (Table 1). This model fit the spectra better than the two temperature model.

Figure 3 shows the best-fit single temperature plus cool-

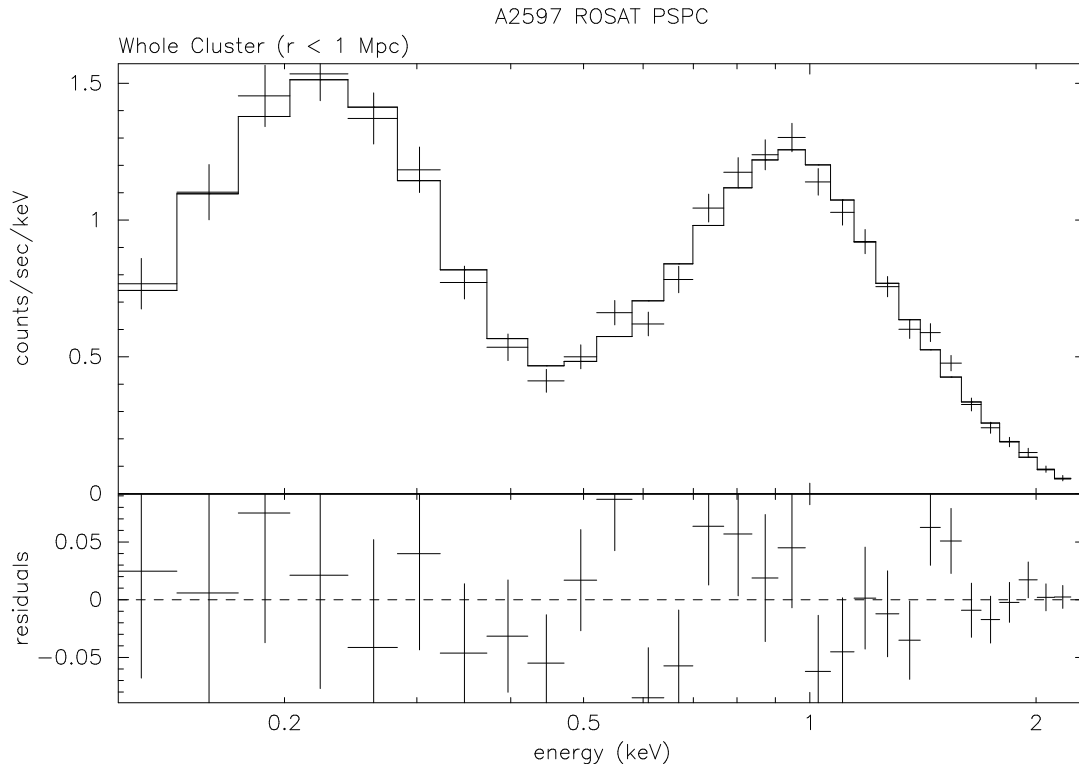


Fig. 3.— The ROSAT PSPC X-ray spectrum for the whole A2597 cluster is compared to the best-fit single temperature plus cooling flow model. The notation is the same as in Figure 2.

ing flow model to the spectrum of the entire cluster. This model provides a considerably improved and acceptable fit to the spectrum of the entire cluster, with $\chi^2 = 27.05$ for 25 d.o.f. Some of the parameters of this model are given in Table 1. In this model, the hydrogen column is well-determined, and the emission measure of the hotter gas and the cooling rate in the cooling flow are moderately well-determined. The temperature of the intracluster gas and its abundances are very poorly determined. We were only able to derive a lower limit for the gas temperature, and the abundance is practically undetermined (the errors allow all sensible values). This is not surprising for several reasons. First, the soft X-ray spectrum of isothermal hot gas depends only weakly on the temperature. Second, the soft X-ray spectrum of isothermal hot gas is nearly independent of the abundances because all of the common elements are fully ionized except iron, and the strong iron lines are at photon energies of about 7 keV. Third, the soft X-ray emission from cooling gas is nearly independent of its initial temperature as long as that temperature is suitably high (Wise & Sarazin 1993). Fourth, the X-ray spectrum of cooling gas is roughly independent of the abundances in the gas because increasing the abundances increases both the emissivity and the cooling rate (e.g., Wise & Sarazin 1993).

The cooling rate derived from the spectrum, $\dot{M} = 344_{-67}^{+75} M_{\odot} \text{ yr}^{-1}$, is in agreement with that derived from analyses of the *Einstein* IPC image ($370 M_{\odot} \text{ yr}^{-1}$; Crawford et al. 1989) and the ROSAT HRI ($327 M_{\odot} \text{ yr}^{-1}$; Paper I).

Because of the effect of the cooling flow at the center of the cluster on the overall spectrum, we determined the

spectrum for the outer intracluster gas in A2597 at projected radii of 250 kpc to 1 Mpc (Table 1). The inner radius of 250 kpc was chosen to be larger than the cooling radius as determined by X-ray surface brightness profiles (Crawford et al. 1989; Paper I), and larger than the region where the spatially resolved spectra, described below, require a cooling flow component. The 90% confidence range for the temperature here (2.28–6.59 keV) is in better agreement with the temperature from *Einstein* MPC measurement. For the reasons given above, the abundance is poorly determined at these higher temperatures, and we have only a lower limit of about 0.43 of cosmic. The single temperature model provided an adequate fit to the outer cluster spectra ($\chi^2 = 31.54$ for 26 d.o.f. The fit was not improved by adding a cooling flow model, and the upper limit on the cooling rate in the outer cluster was $\dot{M} < 39 M_{\odot} \text{ yr}^{-1}$ (90% confidence).

4.2. Spatially-Resolved Spectra

The PSPC X-ray spectra of A2597 were also determined in a set of five circular annuli centered on the central cD galaxy (which is coincident with the peak in the X-ray surface brightness). The widths were determined from the PSPC point-spread-function (PSF) in the inner regions, and by requiring that each spectrum contain at least 1000 net counts in the outer regions. The resulting fits are shown in Table 1. The abundances are not well-determined in any of these spectra, so we adopted a fixed abundance of 0.5 of cosmic. This is consistent with the values from the overall spectrum and the outer cluster spectrum and with the results for other clusters with similar luminosities

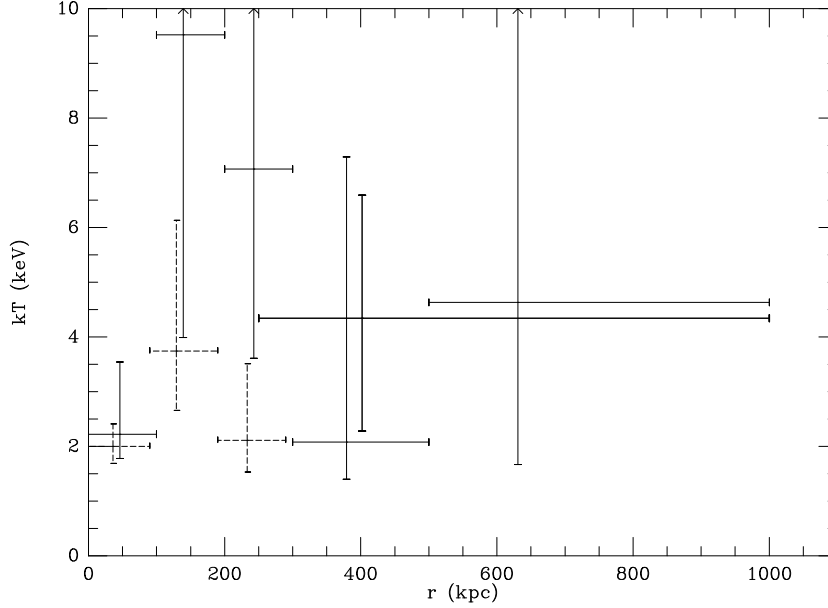


Fig. 4.— The ROSAT PSPC temperature as a function of projected radius from the X-ray spectra in annuli and the outer cluster spectrum. The solid error bars are the best models from Table 1. The temperature from the outer cluster spectrum is shown with a thicker line. The dashed error bars are the single temperature fits for the three inner radii where cooling flow components were required to fit the spectrum. These points were displaced slightly toward the y-axis to separate them from the solid error bars; in fact, they include the same radii. The vertical error bars are 90% confidence intervals; the arrows at the top of the figure indicate temperature values which are only lower limits. The horizontal bars give the widths of the regions over which the spectra were accumulated. Each point was plotted at the median radius for the X-ray emission in that annulus.

Table 1:

ROSAT PSPC X-RAY SPECTRAL FITS							
Region	Single Temperature Model			Single Temperature Plus Cooling Flow			
	N_H (10^{20} cm^{-2})	kT (keV)	$\chi^2/\text{d.o.f.}$	N_H (10^{20} cm^{-2})	kT (keV)	\dot{M} ($M_\odot \text{ yr}^{-1}$)	$\chi^2/\text{d.o.f.}$
Whole Cluster ($r \leq 1 \text{ Mpc}$)	$1.89^{+0.21}_{-0.20}$	$2.61^{+0.68}_{-0.48}$	47.88/26	$1.18^{+0.25}_{-0.15}$	>3.52	344^{+75}_{-67}	27.05/25
Outer Cluster (0.25–1 Mpc)	$1.77^{+0.34}_{-0.30}$	$4.34^{+2.25}_{-2.06}$	31.54/26				
$r \leq 0.1 \text{ Mpc}$	$2.49^{+0.14}_{-0.13}$	$2.00^{+0.41}_{-0.31}$	40.88/27	$2.48^{+0.14}_{-0.14}$	$2.22^{+1.32}_{-0.44}$	92^{+85}_{-92}	38.20/26
0.1–0.2 Mpc	$1.32^{+0.15}_{-0.16}$	$3.74^{+2.39}_{-1.08}$	29.36/27	$1.19^{+0.18}_{-0.12}$	>3.99	81^{+35}_{-35}	22.67/26
0.2–0.3 Mpc	$1.60^{+0.24}_{-0.22}$	$2.11^{+1.40}_{-0.58}$	28.58/25	$1.45^{+0.24}_{-0.22}$	>3.61	58^{+27}_{-49}	24.72/24
0.3–0.5 Mpc	$1.95^{+0.35}_{-0.30}$	$2.08^{+5.21}_{-0.68}$	29.57/27				
0.5–1.0 Mpc	$1.47^{+0.38}_{-0.92}$	>1.67	39.40/26				

(e.g., Edge & Stewart 1991).

The spectra in the inner three annuli ($r \leq 300 \text{ kpc}$) are not well-fit by single temperature models. Because the PSPC spectra of these annuli are generally softer than the *Einstein* MPC cluster spectrum, we have also fit these regions including a cooling flow component. These models are shown at the right of Table 1. When the cooling flow components to the spectrum are included, the ambient gas temperatures in most of the annuli are poorly constrained. Note that the cooling rate in each of the three inner 100 kpc annuli are similar, suggesting that gas is cooling out of the hot intracluster medium over a substantial region of $\sim 250 \text{ kpc}$ in radius. The nearly equal cooling rates

in these annuli are crudely consistent with $\dot{M} \propto r$, as has been suggested for many other cooling flow clusters based on surface brightness data (e.g., Fabian, Nulsen, & Canizares 1991). Note that the cooling rate in the central region is quite uncertain. This is due to the low ambient gas temperature for this region, which means that both of the two spectral components have similarly soft spectra. Thus, the cooling flow component makes a smaller contribution to the ROSAT band, and the ambient gas and cooling flow contributions are strongly anticorrelated.

For two outer annuli (300–1000 kpc), the fit is not improved by the addition of a cooling flow component, and the best-fit cooling rate is zero. Moreover, the cooling rate

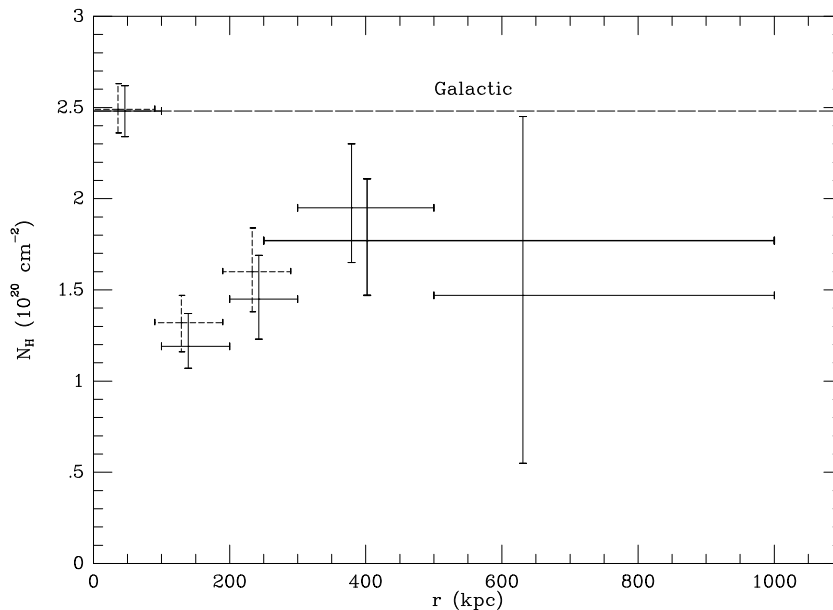


Fig. 5.— The ROSAT PSPC absorbing hydrogen column as a function of projected radius for the X-ray spectra in annuli. The notation is the same as in Figure 4. The dashed horizontal line is the Galactic column from Stark et al. (1992).

for the outer cluster ($r \geq 250$ kpc) is zero. Thus, there is no spectral evidence for cooling beyond about 250 kpc.

The temperatures from the fits to these spectra are plotted in Figure 4. The solid error bars represent either the best single temperature model or the best single temperature plus cooling flow model for the three inner annuli where the single temperature model did not give a good fit. For the three inner annuli, the single temperature model is shown as a dashed error bar. The vertical error bars are 90% confidence intervals. The horizontal bars give the width of the annulus over which the spectrum was accumulated. Each point was plotted at the median radius for the X-ray emission in that annulus. The outer cluster temperature is also shown. There is no clear evidence for a trend in the ambient gas temperature except for the drop within 100 kpc.

The hydrogen columns required to fit the soft X-ray absorption in the PSPC annular spectra are shown in Figure 5. The dashed line is the Galactic value from the 21 cm H I measurements of Stark et al. (1992). Most of the values are somewhat lower than the value from the radio observations. The inclusion of the cooling flow in the inner three spectra doesn't affect the derived columns in a significant way.

4.3. Excess Absorption?

Excess soft X-ray absorption has been found in the *Einstein* SSS spectra of many cooling flow clusters (White et al. 1991). ROSAT PSPC and ASCA spectra have confirmed this absorption in a number of cases (Allen et al. 1993; Fabian et al. 1994), and the ROSAT PSPC spectral images have shown that the excess absorption is confined to the inner cooling regions of the cluster in some cases (Allen et al. 1993; Irwin & Sarazin 1995). A2597 was not included in the sample studied by White et al.; however, for strong cooling flows like A2597, the excess columns were typically $\gtrsim 1 \times 10^{21} \text{ cm}^{-2}$.

Toward A2597, the measured Galactic hydrogen column

is $N_H = 2.45 \times 10^{20} \text{ cm}^{-2}$ (Stark et al. 1992). There is no evidence for other Galactic interstellar matter from the IRAS images of the region. This is a relatively small value, and a significant excess column should be easy to detect compared with this absorption. None of the spectra in Table 1 and Figure 5 require more absorption than the Galactic value, and most require less. An excess absorption column similar to those seen in other similar cluster cooling flows ($\Delta N_H \sim 10^{21} \text{ cm}^{-2}$) can be ruled out with high confidence. Figures 6a,b illustrate this point. Figure 6a shows the best-fit single temperature plus cooling flow model of Table 1 compared to data for the inner 100 kpc of the cluster. Figure 6b compares this to the best-fit model of the same type, but with an excess column of $\Delta N_H = 10^{21} \text{ cm}^{-2}$. The ROSAT PSPC response naturally divides the spectrum into soft and hard bands at about 0.4 keV. In the presence of excess absorption on the order of $\Delta N_H \sim 10^{21} \text{ cm}^{-2}$, the soft band should be strongly suppressed. This is not observed in the central spectrum of A2597 (Fig. 6a). The best-fit model with an excess column of $\Delta N_H = 10^{21} \text{ cm}^{-2}$ has an increase in $\chi^2 = 662$ for one less degree of freedom, and is thus completely excluded.

The central spectrum in Figure 6 was collected from within a projected radius of 100 kpc. Thus, it includes emission from regions at larger radii in front of and behind the cluster core. If there were excess absorption associated with the gas in the core, then it would act only on the emission within and behind the core. This might dilute the effect of the excess absorption. To try to measure or limit the amount of absorption acting on the emission from the cooling core alone, we constructed a spectrum in which the background was taken from the outer annuli, and scaled so as to remove the foreground cluster emission. The scaling was determined from the surface brightness profile of the cluster (§ 5.2). This did produce a somewhat better single temperature fit to the spectrum ($\chi^2 = 36.75$ for 27 d.o.f.) with a lower temperature ($kT = 1.75^{+0.46}_{-0.21}$)

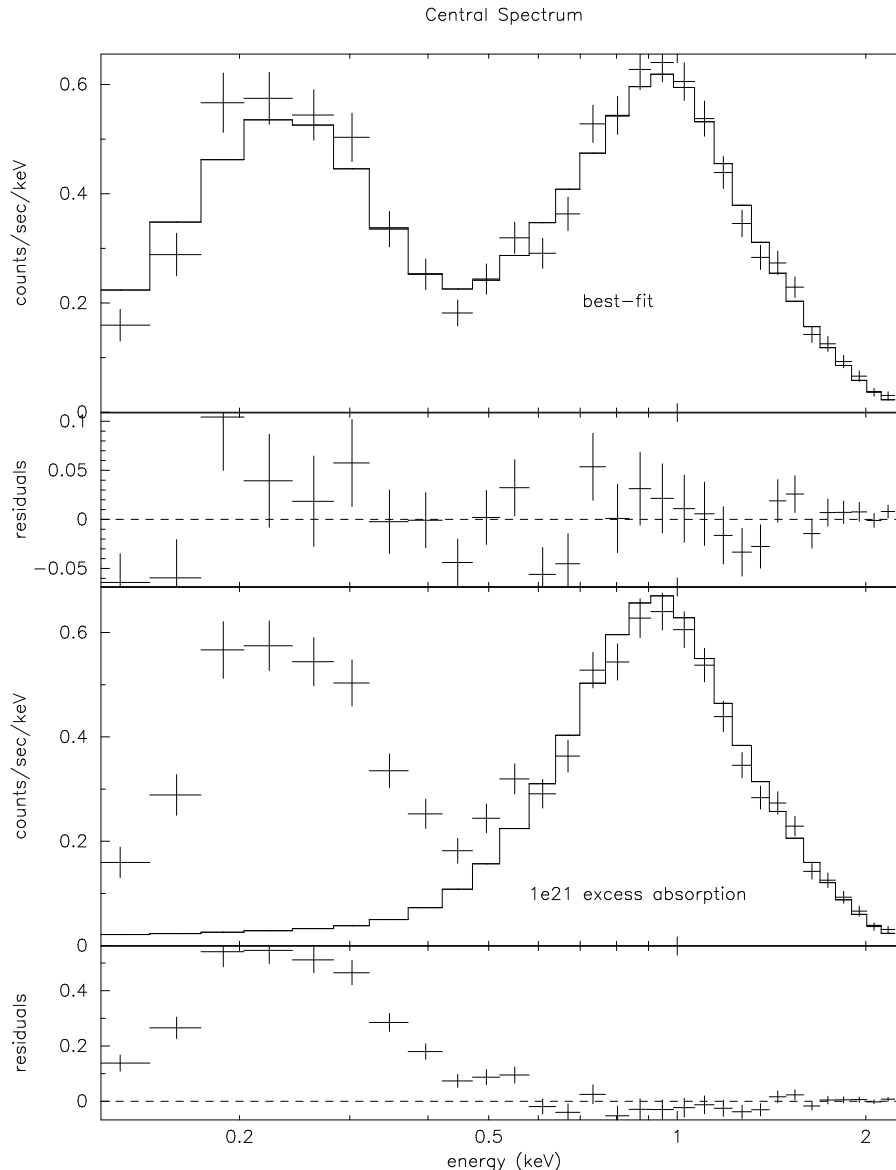


Fig. 6.— (Upper 2 panels): The ROSAT PSPC X-ray spectrum for the central 100 kpc (in projected radius) of the A2597 cluster is compared to the best-fit single temperature plus cooling flow model. The notation is the same as in Figure 2. (Lower 2 panels): The same spectrum, but fit with a model with an excess absorption of $1 \times 10^{21} \text{ cm}^{-2}$.

and a slightly higher absorbing column ($N_H = 2.79^{+0.22}_{-0.20}$). The column was identical in a model with a cooling flow. Since this gave the highest value of the central absorbing column of any of the methods employed, we use this value to set an upper limit on the excess absorption associated with the cluster cooling core. If this value is compared to the measured Galactic column, the difference is $0.54 \times 10^{20} \text{ cm}^{-2}$.

There may be systematic errors in converting the wide-beam H I measurements of Stark et al. (1992) to a total hydrogen column toward the cooling core of A2597. To give more conservative upper limit to the excess, we compare the absorbing column for the single temperature model in front of the cooling core with the value for outer cluster region (Table 1). Note that this outer spectrum should be representative of the foreground absorption in the outer regions of the cluster. The abundances were again fixed at 50% of cosmic. Including the effects of the redshift, the

90% confidence upper limit on the excess absorption column was

$$\Delta N_H < 1.68 \times 10^{20} \text{ cm}^{-2}. \quad (1)$$

Given the assumptions that were made to maximize the value of the excess absorption, this would seem to be an extreme upper limit. Thus, the excess absorption toward A2597 is at least an order of magnitude smaller than typical values toward other similarly large cooling flows (White et al. 1991).

Remarkably, A2597 is one of the few cooling flows toward which a large column has been detected in 21 cm H I absorption (O’Dea et al. 1994a). O’Dea et al. detect two absorption components. A narrow line is seen toward the nucleus with a velocity width of $\approx 220 \text{ km s}^{-1}$ and a column of $N_H^n = 8.2 \times 10^{20} (T_s^n / 100 \text{ K}) \text{ cm}^{-2}$, where T_s is the spin temperature of the hydrogen. This component is not spatially resolved. There is also a broad component with

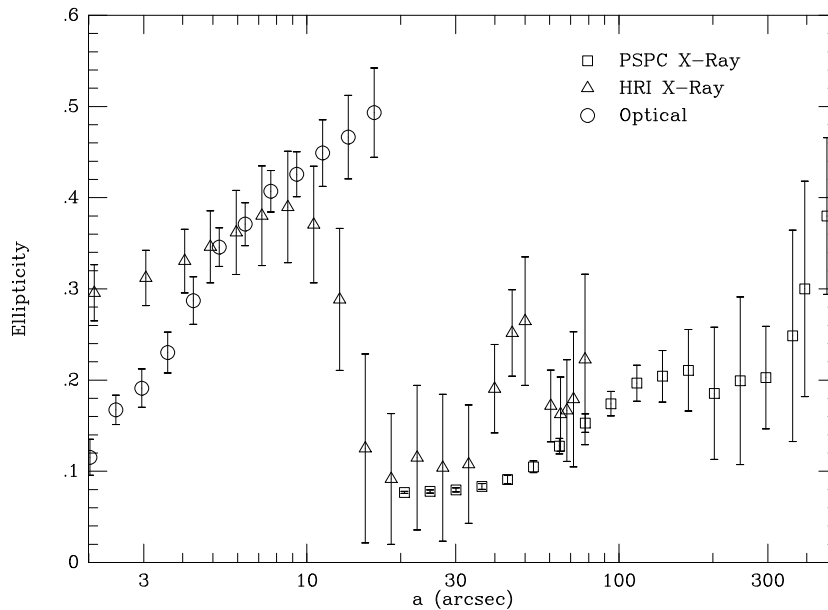


Fig. 7.— The ellipticity of the X-ray and optical isophotes of A2597 are shown as a function of the semimajor axis a of the isophotes. The squares and triangles are from ROSAT PSPC and HRI images, respectively. The HRI data is from Paper I. The circles are from the optical V-band image of the central cD galaxy from McNamara & O’Connell (1993). One σ error bars are shown.

a width of $\approx 410 \text{ km s}^{-1}$ which appears extended over the entire radio source. This broad component has a column of $N_H^b = 4.5 \times 10^{20} (T_s^b/100 \text{ K}) \text{ cm}^{-2}$. O’Dea et al. suggest that the broad component is associated with the optical emission line nebula at the center of the cooling flow.

Is our upper limit on the X-ray absorption consistent with the detected hydrogen in front of the radio source in this cD galaxy? The radio source is extremely small, extending only to a projected radius of $r < 4$ arcsec. The absorption could be greatly diluted over the larger aperture used for the PSPC central spectrum. The PSF of the PSPC does not allow one to determine the spectrum on the scale of the radio source. However, to test the consistency between the X-ray spectrum and the radio data, we compared the X-ray data to a spectral model in which the total column, $N_H = 12.7 \times 10^{20} \text{ cm}^{-2}$, associated with the H I absorption at a spin temperature of $T_s = 100 \text{ K}$ covers the inner 4 arcsec of the X-ray emission. This absorption was in addition to the previously determined absorption (Table 1). This exaggerates the effect of the radio absorption in several ways. First, the narrow 21 cm component is spatially unresolved, and covers a much smaller area. Second, part of the radio absorption was presumably included in the previous spectral fit. The fraction of the X-ray emission from this area is estimated from the surface brightness profile of the ROSAT HRI (§ 5.2; Paper I), corrected for the PSF of the HRI. All other spectral parameters were kept fixed at their previous values (Table 1). This model spectrum could not be distinguished from the previous best-fit model by even $1\text{-}\sigma$. Thus, our X-ray spectra and the upper limit on excess absorption we derived are consistent with the H I absorption detections of O’Dea et al. (1994a).

O’Dea et al. suggest that the broad absorption component is associated with the optical emission line nebula, which covers a much larger projected area of $r < 14$ arcsec (Heckman et al. 1989). For a spin temperature

of 100 K, the broad component has a column density of $N_H^b = 4.5 \times 10^{20} \text{ cm}^{-2}$. Such a column of hydrogen covering the inner 14 arcsec radius of the X-ray emission might be detectable. Simply adding this absorption to the model in Table 1 increases the χ^2 by 27. If one refits the spectrum including this absorption by the broad H I component in the inner 14 arcsec, the foreground column is reduced from 2.49 to $2.07 \times 10^{20} \text{ cm}^{-2}$. The spectral fit is worse by $\Delta\chi^2 = 2.95$, which can be rejected with more than 90% confidence. Thus, the X-ray spectra are moderately inconsistent with the broad component having a column density of $N_H^b = 4.5 \times 10^{20} \text{ cm}^{-2}$ that uniformly covers the entire region of the emission line nebula ($r < 14$ arcsec). A larger region of coverage is certainly ruled out by the upper limit of $2.62 \times 10^{20} \text{ cm}^{-2}$ on the column in the central X-ray spectrum. On the other hand, the spin temperature may be less than 100 K, the abundance of carbon and oxygen (which provide a large part of the X-ray absorption) may be lower than cosmic, or the H I may be centrally condensed (as the H α emission is observed to be) and the neutral column from the radio observation may only apply at the center. It is likely that a centrally condensed distribution of neutral hydrogen similar to the surface brightness of the H α could not be ruled out by our PSPC spectrum.

5. SPATIAL ANALYSIS

5.1. Isophotal Shape

Figure 1 shows that the X-ray emission from A2597 is elongated. We measured the shape of the X-ray image using the best-fit elliptical isophotal model for the X-ray emission. The X-ray surface brightness was assumed to be represented by a series of concentric elliptical isophotes. The centers of the isophotes were fixed at the X-ray centroid, while the ellipticities and position angles of the fitted ellipses were allowed to vary. The elliptical isophotes were

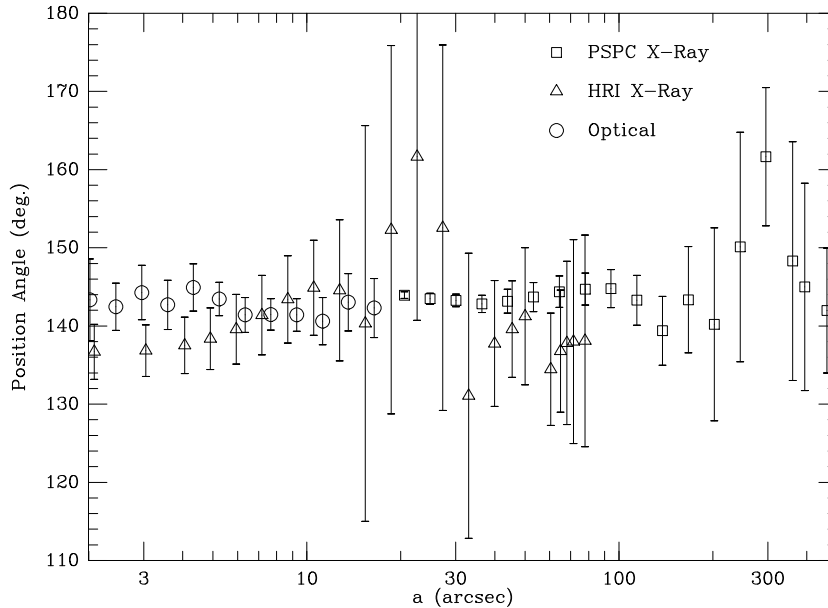


Fig. 8.— The position angles of the X-ray and optical isophotes of cluster A2597 are shown as a function of the semimajor axis a of the isophotes. The position angle is measured from north toward the east. The notation is the same as in Figure 7.

determined using the algorithm of Jedrzejewski (1987). A similar analysis was done previously for the ROSAT HRI image of A2597 (Paper I). For comparison, we determined the ellipticity of the central cD galaxy in A2597 using the V-band image from McNamara & O’Connell (1993) in a similar manner.

Figure 7 shows the ellipticity, ϵ , as a function of the semimajor axis, a , of the elliptical isophotes for the ROSAT PSPC, ROSAT HRI, and optical V-band data. At the smallest semimajor axes plotted for each instrument ($a \lesssim 2''$ in the optical, $a \lesssim 4''$ in the HRI, and $a \lesssim 30''$ in the PSPC), the ellipticity may be reduced somewhat by the instrument PSF. The ROSAT HRI image is strongly elongated ($\epsilon \approx 0.4$) at the center; this was discussed in some detail in Paper I. At larger radii ($a \gtrsim 15$ arcsec), the X-ray ellipticity is much smaller ($\epsilon \approx 0.1$), although it increases to larger radii. The ROSAT PSPC and HRI elongations are consistent where they overlap, except for a narrow range of radii around 45 arcsec. This might be due to a weak, variable X-ray source. The PSPC image becomes fairly elongated at the largest radii for which the shape could be measured with any confidence.

Figure 8 gives the position angle of the semimajor axis (measured north through east) for the three images. We see that the orientation of the X-ray isophotal ellipses remains nearly constant from 2 arcsec out to 500 arcsec. The position angle may increase slightly with radius (from 137° to approximately 145°). The ellipticities of the V-band isophotes of the cD galaxy increase rapidly with radius in the inner 7 arcsec; the ellipticity is nearly constant at values between 0.4–0.5 at larger radii (Figure 7). Increasing ellipticity with radius is a common property of brightest cluster ellipticals (Porter, Schneider, & Hoessel 1991). The isophotal position angles are fairly constant with radius at a value of $\approx 143^\circ$. The isophotal ellipticities and position angles found from our V and I data are concordant, as are those in the Thuan-Gunn R-band by Porter et al. (1991). We have therefore presented only the V-band

data here. Although some of the increasing ellipticity with radius seen in the optical band is probably real, the slope and intercept (central ellipticity and position angle) may be strongly affected by seeing in the inner several arcsec. Franx, Illingworth, & Heckman (1989) showed that optical ellipticities and position angles can be strongly affected (greater than 10%) by the width and shape of the instrument PSF within about 5 times the seeing $FWHM$. The seeing for the V and I band data was $FWHM = 1.6$ arcsec. The position angles of the optical and X-ray data agree to within their uncertainties, and the average optical and X-ray ellipticities within 15 arcsec are similar.

On large scales, the orientation of the galaxy distribution in A2597 is similar to that of the X-ray emission (Trèvese, Cirimele, & Flin 1992a,b). The ellipticity of the galaxy distribution is somewhat larger than that of the X-ray emission, although the errors on both are also quite significant. Buote & Canizares (1996) note that the ellipticity of the mass distribution and galaxy distribution in clusters is expected to exceed that of the X-ray distribution in most cases.

In order to search for substructure within the ROSAT PSPC image of A2597, we constructed a synthetic image of the cluster using the data on the best-fit elliptical isophotes of the cluster in Figures 7 and 8. This was subtracted from the actual image of the cluster in Figure 1, and the significance of any residuals was determined. (This procedure is described in more detail in Paper I.) The only significant positive features were associated with Srcs. 9, 19, 20, 21, and 23 in Table 2, and with two weaker (4σ) sources at R.A. = $23^h24^m43^s.7$ and Dec. = $-12^\circ07'31''$, and R.A. = $23^h25^m56^s.2$ and Dec. = $-12^\circ09'24''$ which are seen at the center right and left of Figure 1. There are a few weak, negative features at the northern and southern ends of the cluster, but other than this, the cluster is very well fit by elliptical isophotes. This suggests that the cluster is well-relaxed and in hydrostatic equilibrium out to projected radii of 1–2 Mpc. In the HRI image of the very center of

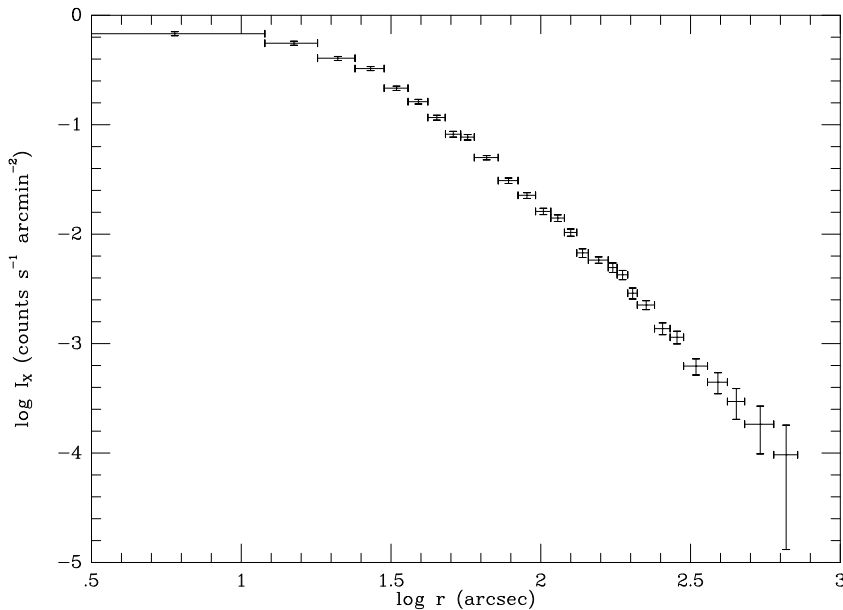


Fig. 9.— The ROSAT PSPC X-ray surface brightness profile of A2597, corrected for background and exposure. This surface brightness in counts $\text{s}^{-1} \text{arcmin}^{-2}$ in the photon energy band of 0.4 – 2.4 keV (PI channels 42–247).

the cluster cooling flow, significant substructures are seen (Paper I). There is an elongated bar of emission which appears partially as the central increase in the ellipticity in Figures 7. There are also some other asymmetries in the emission near the center. These are apparently unresolved in the PSPC image.

5.2. X-Ray Surface Brightness Profile

The azimuthally averaged X-ray surface brightness distribution of the cluster was derived from the ROSAT PSPC counts in circular annuli centered on the X-ray centroid. The photon energy band of 0.4 – 2.4 keV (PI channels 42–247) was used to minimize the background contribution (which is mainly very soft) compared to cluster emission (which is expected to be mainly very hard). Although the X-ray image of the cluster is moderately elliptical (§ 5.1), the use of elliptical annuli with variable ellipticities and/or position angles would make it difficult to deconvolve the gas density from the X-ray surface brightness. In addition to quantities derivable from the observed surface brightness, one would need to specify the third axis of the ellipsoid, and two additional angles. Instead, we use circular annuli. White et al. (1994) have shown that small ellipticities of the order of those in A2597 do not strongly affect the inferred X-ray surface brightness and gas density. In general, the surface brightness of an elliptical isophote corresponds approximately to the azimuthally-averaged surface brightness at a radius equal to the geometric mean of the semimajor and semiminor axes of the ellipse.

The resulting ROSAT PSPC surface brightness profile, corrected for background and exposure, is shown in Figure 9. Point sources have been removed. X-ray emission is detected out to a radius of $1080'' = 18' = 2.37 \text{ Mpc}$. However, the errors in the surface brightness are very large beyond $12' = 1.58 \text{ Mpc}$, and we only include data within this radius in Figure 9.

At smaller radii, the ROSAT HRI spatial resolution is

better. Because of the longer exposure in the HRI, the counts in the central regions of the image are similar, and so the errors in the surface brightness there are similar. At large radii, the lower background in the PSPC provides a better determination of the X-ray surface brightness. At intermediate radii (1–4 arcmin), the HRI and PSPC give consistent results. To take advantage of the better resolution of the HRI at small radii and the lower background of the PSPC at larger radii, we have merged the two profiles into a single X-ray surface brightness profile. We adopt the HRI profile for projected radii $r < 108 \text{ arcsec}$ and the PSPC profile for projected radii $r > 108 \text{ arcsec}$. (The HRI profile was published previously in Paper I.) To match the two, we converted the count rate in the HRI to the equivalent value in the PSPC, we adopted the region from 200–300 kpc and determined the conversion from the instrument responses, assuming the best-fit single temperature spectrum for this region from Table 1. The counting rate was converted into a physical flux assuming the best-fit single temperature spectrum for the entire cluster (Table 1). However, the adopted spectra have little actual affect on the scaling of HRI to PSPC counts or the conversion to physical flux. The X-ray surface brightness profile is shown as the upper points in Figure 10 with 1σ errors.

We fitted the X-ray surface brightness in Figure 10 with the isothermal “beta” model, $I_X(r) = I_o[1 + (r/r_{\text{core}})^2]^{-3\beta+1/2}$. When all of the data points in Figure 10 were included, the best-fit values were $r_{\text{core}} = 21 \pm 2 \text{ arcsec}$ and $\beta = 0.59 \pm 0.09$, but the fit was not acceptable (minimum $\chi^2 = 59.99$ for 29 d.o.f.). As had generally been found with cooling flows clusters (e.g., Jones & Forman 1984), the beta model could not fit the sharply peaked central surface brightness within the cooling radius. We tried a number of simple models for the cooling flow portion of the X-ray surface brightness profile, but none gave an acceptable fit. Instead, we fit the surface brightness with the beta model, progressively removing the interior points until an acceptable fit was found. This required the

removal of the data points interior to a projected radius of 84 arcsec (180 kpc). This is similar to the cooling radius in the cluster (Crawford et al. 1989; Paper I). With these interior points removed, an acceptable beta model fit was found ($\chi^2 = 12.88$ for 14 d.o.f.), which gave $\beta = 0.64^{+0.08}_{-0.03}$ (90% confidence). Note that this value of β is consistent, within the errors, with that found from the unacceptable fit including all of the data points. This is not surprising, as the value of β is mainly constrained by the decline in the X-ray surface brightness at large radii, and the data points at large radii were included in both fits. The fit excluding the central points gave only an upper limit to the core radius, $r_{core} < 78$ arcsec (90% confidence). Again, this upper limit on the core radius includes the value found in the unacceptable fit including all of the data points. Thus, it seems fair to conclude that the centrally peaked X-ray emission due to cooling flow makes it impossible to determine the core radius of the cluster, and that the data only allow an upper limit of $r_{core} < 78$ arcsec (170 kpc). On the other hand, the value of β is well-determined, and the behavior of the surface brightness at large radii is consistent with the beta model. The best-fit beta model, excluding the central points, is shown as a solid curve in Figure 10. A de-projection of the surface brightness of the cooling flow region was given previously in Paper I.

Based on numerical simulations of clusters, Navarro, Frenk, & White (1995) and Bartelmann & Steinmetz (1996) suggest that the actual density profiles of the intracluster gas steepen as compared to the beta model fits. Figure 10 doesn't show any evidence for this, but our data may not extend to a large enough radius.

The X-ray emissivity of the gas was determined by de-projecting the X-ray surface brightness into spherical shells, each of constant emissivity (e.g., Arnaud 1988). The electron density was then determined and is plotted as the lower points in Figure 10.

6. GAS AND TOTAL MASS PROFILES

The values of the electron density from Figure 10 were integrated over the volume to give the profile of the gas mass interior to the radius $M_{gas}(r)$ (Figure 11). The total gravitational mass was determined from the assumption that the gas is in hydrostatic equilibrium. This implies that the total gas mass interior to each radius is given by

$$M_{tot}(r) = -\frac{r^2}{G\rho_{gas}} \frac{dP}{dr}, \quad (2)$$

where P and ρ_{gas} are the gas pressure and density, respectively. The gas density ρ_{gas} was taken from Figure 10. To determine the gas pressure, we need to know the gas temperature as a function of radius in the cluster. The gas temperature as a function projected radius is shown in Figure 4 as derived from the PSPC spectra. It is clear that the errors are very large, and that the temperature is very poorly constrained in the inner points where there is a contribution to the spectrum from a cooling flow. There is no clear evidence for a radial trend in the temperatures, except for the drop in temperature within the inner 100 kpc. Thus, we have assumed a constant value for the temperature set by the outer cluster spectrum, $kT = 4.34^{+2.25}_{-2.06}$ keV. The errors in the masses were assessed using Monte

Carlo simulations of the X-ray surface brightness data to determine the 90% confidence region, including the errors on the temperature in each data point individually. Note, however, that the errors for the points are correlated in a complex manner, both because of the de-projection of the surface brightness and of the inclusion of the error in the overall cluster temperature separately in the error in the mass at each radius. Obviously, ASCA spectra of A2597 would be of great value in determining the temperature profile more accurately.

For comparison, we also determined the gas and total masses for the best-fit beta-model surface brightness fits for the gas distribution. We used the best-fit model using all of the surface brightness points, including the central excess emission in the cooling flow. The resulting mass profiles for the best-fit model are the solid curves in Figure 11. The de-projection densities are not corrected for the effects of the finite instrument PSF, and this causes the de-projection to give different results than the best-fit beta-model (which is corrected for the PSF) for the innermost points.

The mass profiles for the best-fit beta-model give $M_{gas} = 1.2 \times 10^{14} M_{\odot}$ and $M_{tot} = 5.6 \times 10^{14} M_{\odot}$ at $r = 2$ Mpc, for a gas mass fraction of about 21%. Similarly, the values at a radius of $r = 1$ Mpc are $M_{gas} = 5.0 \times 10^{13} M_{\odot}$ and $M_{tot} = 2.8 \times 10^{14} M_{\odot}$, so that $M_{gas}/M_{tot} = 18\%$. The uncertainty in the spectrally-determined temperatures mean that the values of the total mass are quite uncertain (by at least a factor of two). The gas masses are more accurately known. For example, if we assume that the gas is isothermal at a temperature of 9.1 keV (David et al. 1993), then the gas mass would be increased by about 6%, while the total mass would increase by a factor of 2.1.

7. CONCLUSIONS

We have presented an analysis of the ROSAT PSPC and HRI X-ray observations of the cooling flow cluster A2597. The X-ray emission from the cluster extends to at least 2 Mpc. The X-ray image of A2597 is moderately elliptical, and is elongated in the same direction as optical image of the central cD galaxy and the galaxy distribution in the cluster. The ROSAT PSPC X-ray image is well-represented by regular elliptical isophotes, suggesting that the cluster is reasonably relaxed and in hydrostatic equilibrium.

We analyzed the ROSAT PSPC X-ray spectra of the cluster. Both the overall cluster spectrum and the spatially resolved spectra within 300 kpc require the presence of both hot and cool components. The cool component is fit reasonably by a cooling flow spectral model. The spectrally determined total cooling rate of $\dot{M} = 344^{+75}_{-67} M_{\odot} \text{ yr}^{-1}$ is in good agreement with those derived from analyses of the *Einstein* IPC ($370 M_{\odot} \text{ yr}^{-1}$; Crawford et al. 1989) and the ROSAT HRI ($327 M_{\odot} \text{ yr}^{-1}$; Paper I) X-ray surface brightness profiles. The spatially resolved X-ray spectra indicate that the cooling component is distributed over the inner 300 kpc in radius of the cluster, with significant amounts of gas cooling in the outer parts of this range. This is in reasonably good agreement with the results of analyses of the X-ray surface brightness distribution of the cluster (Crawford et al. 1989; Paper I), and with the general result that gas cools in an extended region in other

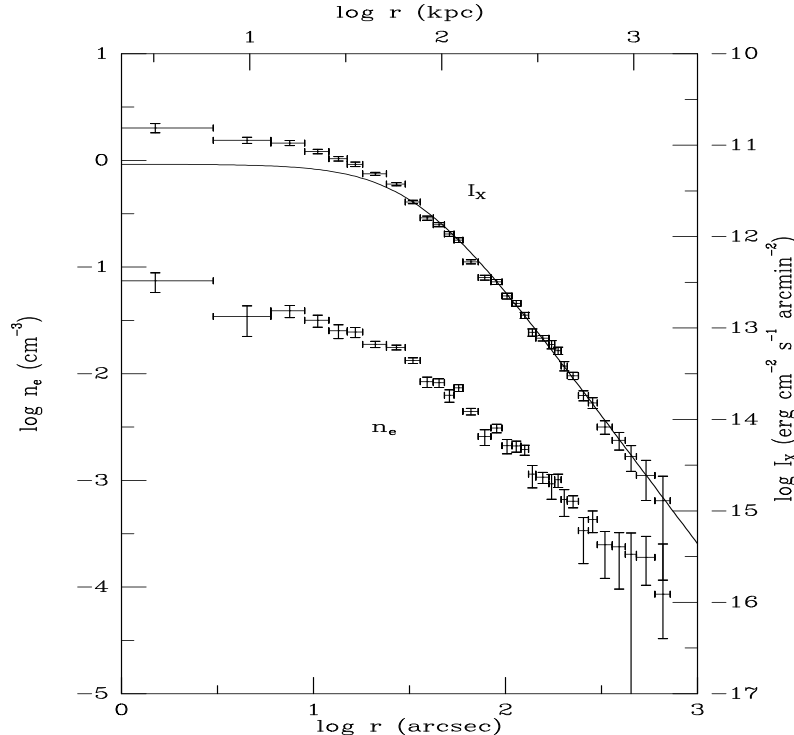


Fig. 10.— The merged ROSAT PSPC and HRI X-ray surface brightness profile and de-projected electron density for A2597. The upper data points give the azimuthally averaged X-ray surface brightness in the band of 0.4 – 2.4 keV as incident at the Earth, corrected for absorption. The scale I_X is given on the right-hand axis. The best beta model fit, excluding data in the inner 84 arcsec, is shown as the solid curve. The lower data points give the de-projected electron number density; the scale is given on the left-hand axis. For each curve, the vertical error bars give the 1σ errors. Note that the deconvolution causes the errors in the electron density values to be correlated. The radial error bars show the widths of the annuli. The lower axis gives the radial scale in seconds of arc, while the upper axis gives the scale in kpc.

cooling flow clusters (e.g., Fabian, Nulsen, & Canizares 1991).

If the cooling flow component is not included in the fits to the ROSAT PSPC spectra, the fits are generally poor and the gas temperatures are too low to be consistent with the *Einstein* MPC spectrum of the entire cluster (David et al. 1993). When the cooling flow component is included, the gas temperature is poorly constrained but generally consistent with the MPC value. As a result, the ROSAT PSPC spectra do not lead to an accurate profile of the variation of the ambient cluster gas temperature with radius. Hopefully, ASCA spectra will provide this information.

We do not detect any significant excess absorption toward the center of A2597. We find a very conservative upper limit of the excess absorbing column at the cluster cooling flow to be $\Delta N_H < 1.72 \times 10^{20} \text{ cm}^{-2}$.

Remarkably, A2597 is one of the few cooling flows toward which a large column has been detected by 21 cm H I radio observations (O’Dea et al. 1994a). O’Dea et al. detect a total column of $\Delta N_H \approx 1 \times 10^{21} \text{ cm}^{-2}$ in absorption against the central radio source in the inner 10 kpc of the cD galaxy in A2597. Our X-ray upper limit is consistent with the detection by O’Dea et al. if the absorber only covers the small region occupied by the radio source.

We determined the ROSAT PSPC radial X-ray surface brightness profile and merged this with the previous ROSAT HRI profile for the inner regions (Paper I).

The profile is not adequately fit by a beta model because of the central X-ray surface brightness peak associated with the cooling flow. If the central 108 arcsec in radius are excluded, the fit becomes acceptable. This fit gave $\beta = 0.64^{+0.08}_{-0.03}$ but only an upper limit to the core radius, $r_{\text{core}} < 78 \text{ arcsec}$ (both 90% confidence). We de-projected the merged X-ray surface brightness to determine the profile of gas density as a function of radius. The hydrostatic equilibrium condition was used to determine the total gravitational mass as a function of radius in the cluster. The gas density was integrated to give the gas mass as a function of radius. Within a radius of 2 Mpc, we found masses of $M_{\text{gas}} = 1.2 \times 10^{14} M_\odot$ and $M_{\text{tot}} = 5.6 \times 10^{14} M_\odot$, and a gas mass fraction of about 21% (for a cluster gas temperature of 4.34 keV). However, our poor knowledge of the spatial variation of the gas temperature makes the total mass values quite uncertain.

C. L. S. was supported in part by NASA ROSAT grants NAG 5–1891, NAG 5–3308, NASA ASCA grant NAG 5–2526, and NASA Astrophysical Theory Program grant 5–3057. B. R. M. received partial support from grant NAS8–39073. C. L. S. thanks Chris O’Dea for useful discussions, and for communicating his results on the 21 cm absorption prior to publication. C. L. S. thanks Zhenping Huang and Jimmy Irwin for helpful advice. C. L. S. and B. R. M. thank an anonymous referee for a number of helpful

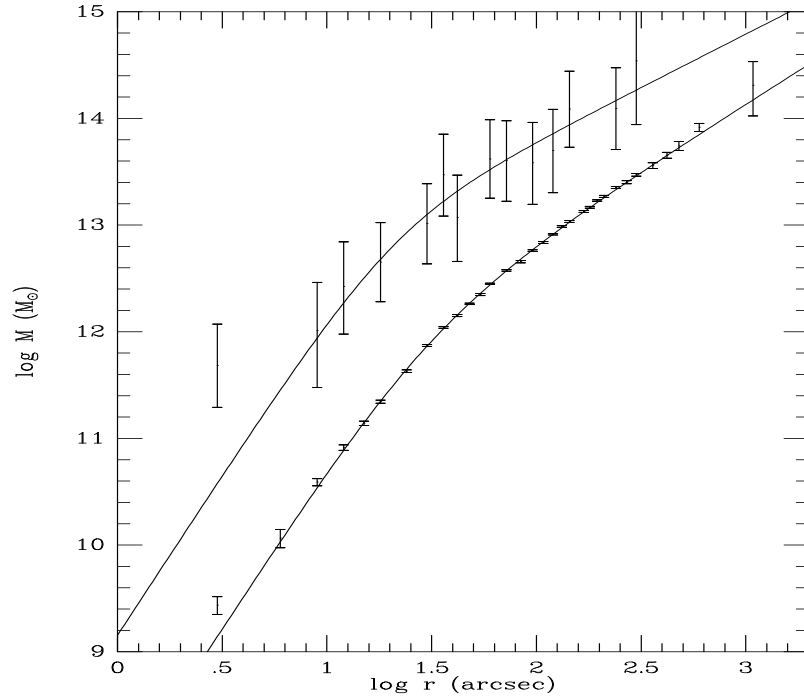


Fig. 11.— The profile of the gas masses (lower) and total gravitational masses (upper) as derived from the ROSAT merged PSPC and HRI X-ray surface brightness profile Fig. 10. The data points give the masses derived from the deconvolved gas density points in Fig. 10. For the total mass (upper points), some of gas density points were combined into larger bins to give a monotonically decreasing pressure profile. Note that the deconvolution causes the error in the masses to be correlated for both the gas mass and total mass. The solid curves are the masses found assuming the best-fit beta-model X-ray surface brightness profile for the cluster (§ 5.2).

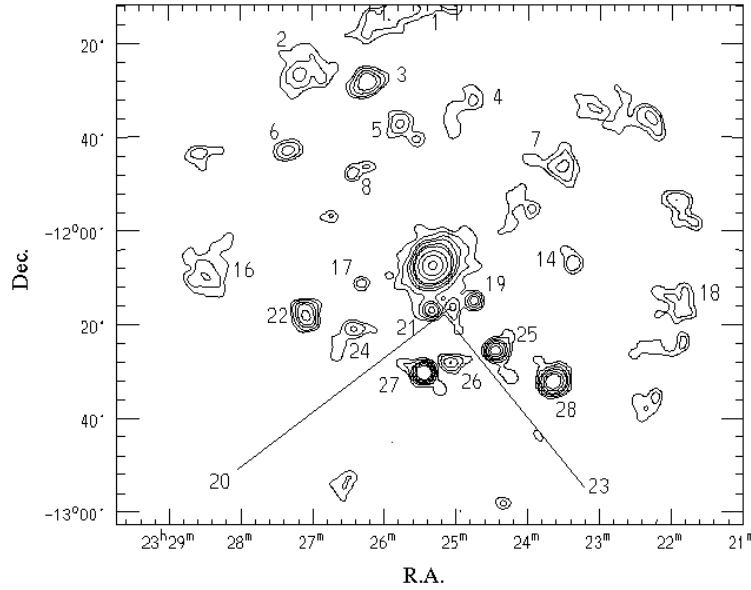


Fig. 12.— A contour plot of the X-ray surface brightness of the entire field of view of the ROSAT PSPC image of A2597. The contours are $(0.7, 1, 1.5, 2, 3, 4, 10, 30, 100) \times 10^{-3} \text{ cts sec}^{-1} \text{ arcmin}^{-2}$ in the 0.1 – 2.1 keV ROSAT band. The image has been adaptively smoothed to a signal-to-noise of five per smoothing beam. The individual X-ray sources outside of the central cluster region are labeled with their numbers from Table 2. The coordinates are J2000.

comments and suggestions.

Table 2:

FIELD X-RAY SOURCES						
Src. No.	R.A. (J2000) (h:m:s)	Dec. (°:':")	Count Rate (10^{-3} s^{-1})		D (arcmin)	Possible ID
			PSPC	HRI		
1	23:25:56.7	-11:15:01	75.3 ^a		53	GD 1148 ?
2	23:27:08.5	-11:27:15	14.2 ^a		47	HD 220826 ?
3	23:26:14.0	-11:28:14	24.7 ^a		41	
4	23:24:46.5	-11:31:27	20.0 ^a		37	
5	23:25:46.7	-11:36:58	17.6 ^a		30	HD 220687
6	23:27:20.5	-11:42:50	19.1 ^a		37	
7	23:23:30.9	-11:46:21	13.7 ^a		34	
8	23:26:27.3	-11:47:38	12.0 ^a		25	
9	23:25:25.5	-12:04:08	18.5±1.9	Y	3	Fluct?
10	23:25:15.4	-12:05:52	N	2.4±0.5	1	Fluct?
11	23:25:15.8	-12:06:30	N	6.5±0.7	1	Fluct?
12	23:25:21.9	-12:06:54	N	13.2±0.9	1	Fluct?
13	23:25:17.9	-12:06:55	N	25.2±1.2	1	Fluct?
14	23:23:22.8	-12:07:20	11.5 ^a		29	
15	23:25:19.1	-12:08:50	Y	3.8±0.6	2	Fluct?
16	23:28:28.8	-12:09:07	35.3 ^a		45	
17	23:26:17.3	-12:11:06	6.1±1.2	Y	14	
18	23:22:01.2	-12:14:43	27.4 ^a		50	HD 220188
19	23:24:44.9	-12:14:52	15.0±1.6	3.3±0.7	11	
20	23:25:02.9	-12:16:13	7.4±1.2	2.9±0.7	10	
21	23:25:19.9	-12:17:06	16.5±1.8	4.3±0.7	9	
22	23:27:04.8	-12:18:22	32.2 ^a		27	
23	23:25:01.2	-12:18:31	4.0±1.0	N	12	
24	23:26:25.4	-12:20:46	10.4 ^a		21	
25	23:24:27.3	-12:25:37	24.4 ^a		22	PHL 5776 ?
26	23:25:03.7	-12:28:45	10.2 ^a		22	PHL 5785 ?
27	23:25:27.0	-12:30:25	76.6 ^a		23	HD 220628
28	23:23:38.5	-12:32:20	60.2 ^a		35	

^aThese sources have very uncertain fluxes because of either their proximity to a rib or their distance from the center of the observing field.

A. APPENDIX — FIELD X-RAY SOURCES

Figure 12 gives a contour plot of the X-ray image of essentially the entire field of view in the photon energy band 0.1 – 2.1 keV (PI channels 11–201). This image was smoothed with an adaptive kernel routine which convolved the image such that each smoothing beam had a minimum signal-to-noise ratio of five; the minimum smoothing length was defined by the PSPC point-spread-function (Huang & Sarazin 1996). The cluster is at the center of the image. Regions of low exposure near the edge of the image were eliminated. Some of the features at the circular edge of the field of view of the telescope are enhanced by the large vignetting and exposure corrections there, and may be spurious.

Maximum-likelihood and local detection algorithms were used to detect point sources in the PSPC and HRI images. A detection criterion of 5σ was adopted. Table 2 gives a list of the sources detected in either the PSPC or the HRI (excluding the extended source associated with A2597 itself). The sources outside of the crowded central region are also labeled in Figure 12. For each source, the table gives its centroid position, its count rate (corrected for background and vignetting) in the PSPC and/or HRI, its projected distance D from the center of the X-ray im-

age, and a comment on the identification. The sources at large distances from the center of the field or near the detector ribs have poorly determined fluxes and positions. None of the sources was clearly extended; however, for sources far from the center of the field where the instrumental point-spread-function is very broad, the upper limits on their size are large.

Only three sources (Src. 19, 20, and 21) were detected clearly in both the HRI and PSPC. Because the HRI has a smaller field of view, sources at large distances from the center of A2597 were only visible in the PSPC. For the region of overlapping coverage, we examined the HRI image at the position of the PSPC sources (and vice versa). We indicate in the table if an enhancement was detected at the position of the source in the other detector (Y) or not (N). A Y indicates that an enhancement is seen, but that it did not satisfy the 5σ detection criteria, either because it was too faint, or resolved out, or possibly varied with time. A number of sources were observed with the HRI near the cluster core which may well just be fluctuations in the surface brightness of the cluster emission; these are noted in the Possible ID column of the Table. Some other possible identifications are noted. Based on the positional errors and the X-ray to optical flux ratios, only the identifications of Srcs. 5, 18, and 27 seem likely to be correct.

REFERENCES

- Abell, G. O., Corwin, H. G., & Olowin, R. P. 1989, *ApJS*, 70, 1
 Allen, S. W., Fabian, A. C., Johnstone, R. M., White, D. A., Daines, S. J., Edge, A. C., & Stewart, G. C. 1993, *MNRAS*, 262, 901
 Antonucci, R., & Barvainis, R. 1994, *AJ*, 107, 448
 Arnaud, K. A. 1988, in *Cooling Flows in Clusters & Galaxies*, ed. A. C. Fabian (Kluwer: Dordrecht), 31
 Ball, R., Burns, J. O., & Loken, C. 1993, *AJ*, 105, 53
 Bartelmann, M., & Steinmetz, M. 1996, preprint astro-ph/9603101
 Böhringer, H., Voges, W., Fabian, A. C., Edge, A. C., & Neumann, D. M. 1993, *MNRAS*, 264, L25
 Buote, D. A., & Canizares, C. R. 1996, *ApJ*, 457, 565
 Buote, D. A., & Tsai, J. C. 1996, *ApJ*, 458, 27
 Crawford, C. S., Arnaud, K. A., Fabian, A. C., & Johnstone, R. M. 1989, *MNRAS*, 236, 277
 Crawford, C. S. & Fabian, A. C. 1992, *MNRAS*, 259, 265
 David, L. P., Slyz, A., Jones, C., Forman, W., Vrtilek, S. D., & Arnaud, K. A. 1993, *ApJ*, 412, 479
 Edge, A. C., & Stewart, G. C. 1991, *MNRAS*, 252, 414
 Fabian, A. C., Arnaud, K. A., Bautz, M. W., & Tawara, Y. 1994, *ApJ*, 436, L63
 Fabian, A. C., Nulsen, P. E. J., & Canizares, C. R. 1991, *A&AR*, 2, 191
 Franx, M., Illingworth, G., & Heckman, T. 1989, *AJ*, 98, 538
 Harris, D. E., Carilli, C. L., & Perley, R. A. 1994, *Nature*, 367, 713
 Heckman, T. M., Baum, S. A., van Bruegel, W. J., & McCarthy, P. J. 1989, *ApJ*, 338, 48
 Hu, E. M. 1988, in *Cooling Flow in Clusters and Galaxies*, ed. A. C. Fabian, (Dordrecht: Reidel), 73
 Hu, E. 1992, *ApJ*, 391, 608
 Huang, Z., & Sarazin, C. L. 1996, *ApJ*, 461, in press
 Irwin, J. A., & Sarazin, C. L. 1995, *ApJ*, 455, 497
 Jedrzejewski, R. 1987, *MNRAS*, 226, 747
 Jones, C. & Forman, W. 1984, *ApJ*, 276, 38
 McNamara, B. R., & Jaffe, W. 1993, *A&A*, 282, 673
 McNamara, B. R., & O'Connell, R. W. 1993, *AJ*, 105, 417
 Morrison, R., & McCammon, D. 1983, *ApJ*, 270, 119
 Navarro, J. F., Frenk, C. S., & White, S. D. 1995, *MNRAS*, 275, 720
 O'Dea, C. P., Baum, S. A., & Gallimore, J. F. 1994a, *ApJ*, 436, 669
 O'Dea, C. P., Baum, S. A., Maloney, P. R., Tacconi, L. S., & Sparks, W. B. 1994b, *ApJ*, 422, 467
 Owen, F. N., White, R. A., & Burns, J. O. 1992, *ApJS*, 80, 501
 Plucinsky, P. P., Snowden, S. L., Briel, U. G., Hasinger, G., & Pfeffermann, E. 1993, *ApJ*, 418, 519
 Porter, A. C., Schneider, D. P., & Hoessel, J. G. 1991, *AJ*, 101, 1561
 Raymond, J. C., & Smith, B. W. 1977, *ApJS*, 35, 419
 Sarazin, C. L., Baum, S. A., & O'Dea, C. P. 1995a, *ApJ*, 451, 125
 Sarazin, C. L., Burns, J., Roettiger, K., & McNamara, B. R. 1995b, *ApJ*, 447, 559 (Paper I)
 Snowden, S. L. 1995, *Cookbook for Analysis Procedures for ROSAT XRT/PSPC Observations of Extended Objects and the Diffuse Background* (Greenbelt: NASA USRSDC)
 Stark, T., et al. 1992, *ApJS*, 79, 77
 Trèvese, D., Cirimele, G., & Flin, P. 1992a, *AJ*, 104, 935
 Trèvese, D., Flin, P., Migliori, L., Hickson, P., Pittella, G. 1992b, *A&AS*, 94, 327
 Voit, G. M., & Donahue, M. 1995, *ApJ*, 452, 164
 White, D. A., Fabian, A. C., Allen, S. W., Edge, A. C., Crawford, C. S., Johnstone, R. M., Stewart, G. C., & Voges, W. 1994, *MNRAS*, 269, 589
 White, D. A., Fabian, A. C., Johnstone, R. M., Mushotzky, R. F., & Arnaud, K. A. 1991, *MNRAS*, 252, 72
 Wise, M. W., & Sarazin, C. L. 1993, *ApJ*, 415, 58